Structure–property relationships for wet dentin adhesive polymers

Article *in* Biointerphases · December 2018

DOI: 10.1116/1.5058072

Structure–property relationships for wet dentin adhesive polymers

Ranganathan Parthasarathy, Anil Misra, Linyong Song, Qiang Ye, and Paulette Spencer

Citation: Biointerphases **13**, 061004 (2018); doi: 10.1116/1.5058072
View online: https://doi.org/10.1116/1.5058072
View Table of Contents: http://avs.scitation.org/toc/bip/13/6
Published by the American Vacuum Society

Structure–property relationships for wet dentin adhesive polymers

Ranganathan Parthasarathy,[1,a)] Anil Misra,[2,b)] Linyong Song,[3,c)] Qiang Ye,[4,d)] and Paulette Spencer[5,e)]
[1]*Department of Civil and Architectural Engineering, Tennessee State University, 3500 John A Merritt Blvd, Nashville, Tennessee 37209*
[2]*Department of Civil and Environmental Engineering, Institute for Bioengineering Research, University of Kansas, 5104B Learned Hall, 1530 W 15th Street, Lawrence, Kansas 66045*
[3]*Institute for Bioengineering Research, University of Kansas, 5104A Learned Hall, 1530 W 15th Street, Lawrence, Kansas 66045*
[4]*Institute for Bioengineering Research, University of Kansas, 5101E Learned Hall, 1530 W 15th Street, Lawrence, Kansas 66045*
[5]*Department of Mechanical Engineering, Institute for Bioengineering Research, University of Kansas, 3111 Learned Hall, 1530 W 15th Street, Lawrence, Kansas 66045*

(Received 16 September 2018; accepted 28 November 2018; published 17 December 2018)

Dentin adhesive systems for composite tooth restorations are composed of hydrophilic/hydrophobic monomers, solvents, and photoinitiators. The adhesives undergo phase separation and concomitant compositional change during their application in the wet oral environment; phase separation compromises the quality of the hybrid layer in the adhesive/dentin interface. In this work, the adhesive composition in the hybrid layer can be represented using the phase boundaries of a ternary phase diagram for the hydrophobic monomer/hydrophilic monomer/water system. The polymer phases, previously unaccounted for, play an important role in determining the mechanical behavior of the bulk adhesive, and the chemomechanical properties of the phases are intimately related to the effects produced by differences in the hydrophobic–hydrophilic composition. As the composition of the polymer phases varies from hydrophobic-rich to hydrophilic-rich, the amount of the adsorbed water and the nature of polymer–water interaction vary nonlinearly and strongly correlate with the change in elastic moduli under wet conditions. The failure strain, loss modulus, and glass transition temperature vary nonmonotonically with composition and are explained based upon primary and secondary transitions observed in dynamic mechanical testing. Due to the variability in composition, the assignment of mechanical properties and the choice of suitable constitutive models for polymer phases in the hybrid layer are not straightforward. This work investigates the relationship between composition and chemomechanical properties of the polymer phases formed on the water-adhesive phase boundary using quasistatic and dynamic mechanical testing, mass transfer experiments, and vibrational spectroscopy. *Published by the AVS.* https://doi.org/10.1116/1.5058072

I. INTRODUCTION

Since the composite material is too viscous to establish a direct bond with the tooth, a low-viscosity adhesive is required at the tooth/composite interface. Tooth surfaces, e.g., enamel and dentin, are acid-etched to prepare them for adhesive bonding. With the wet-bonding technique, acid-etching removes the dentin's mineral phase without altering the collagen matrix. The resulting voids in the water-laden collagen matrix are filled with adhesive that undergoes *in situ* polymerization to create the hybrid layer.[1]

The ideal hybrid layer would be a polymerized 3D polymer/collagen network that provides a continuous and stable link between the adhesive and the dentin. Studies indicate that this ideal is not achieved[2–7]—the hybrid layer retains water-rich pockets of resin-sparse collagen fibrils as well as pockets of poorly polymerized hydrophilic-rich adhesive.

The low-viscosity adhesive that bonds the composite to the tooth is intended to seal the interface but the adhesive degrades, which can breach the composite/tooth margin.[8,9] Bacteria and bacterial by-products such as acids and enzymes infiltrate these marginal gaps,[10,11] and the composite's inability to increase the interfacial pH facilitates cariogenic and aciduric bacterial outgrowth.[12,13] Together, these characteristics encourage recurrent decay, pulpal damage, and composite failure.[14,15] The lack of effective and durable dentin adhesives is generally considered as one of the major problems with the use of composites in direct restorative dentistry.[16,17]

A. Commercial dentin adhesives

Commercial dentin adhesive systems are composed of hydrophilic and hydrophobic monomers,[18,19] solvents, and photoinitiators. In the monomer state, the adhesive must be hydrophilic enough to achieve integration with the wet, demineralized dentin matrix. The polymerized adhesive, on the other hand, must be relatively hydrophobic to avoid

[a)]Author to whom correspondence should be addressed: rparthas@tnstate.edu
[b)]Electronic mail: amisra@ku.edu
[c)]Electronic mail: leonsong@ku.edu
[d)]Electronic mail: yeq@ku.edu
[e)]Electronic mail: pspencer@ku.edu

swelling and sorption of oral fluids. To provide durable function in the mouth, the optimal dentin adhesive must possess a hydrophilic/hydrophobic balance.[20] In this paper, we study dentin adhesive systems formed using the hydrophilic/hydrophobic comonomers 2-hydroxyethyl-methacrylate (HEMA)/bisphenol A glycerolate dimethacrylate (BisGMA), which are major components in commercial dentin adhesives.

Adhesive infiltration into the wet demineralized dentin (collagen matrix) may take place by phenomena such as spontaneous diffusion and advection resulting from external energy during application. Since the hydrophobic component BisGMA is more viscous, it transports slower through both diffusion and advection, as compared to the hydrophilic component.[21] In the wet, oral environment, the hydrophilic/hydrophobic monomer composition of these dentin adhesives can experience phase separation[22,23] which compromises the quality of the hybrid layer. Subsequent photopolymerization results in an adhesive–collagen hybrid layer where the composition of the adhesive varies spatially in the hybrid layer.[7,24–28] Since adhesive penetration in the hybrid layer may take place by a combination of diffusion and advection, the adhesive composition is likely represented by the phase boundary on the ternary phase diagram.[29]

A schematic of the adhesive/dentin (a/d) interface and the hybrid layer for a primary molar with a class II composite restoration is shown in Figs. 1(a) and 1(b). The neat resins have been represented on the ternary phase diagram using squares as shown in Fig. 1(c). The black arrow indicates the direction of increasing BisGMA content in the resin.

B. Structure/property relationships of the adhesive/dentin interface

Based upon microscale structure–property measurements, our group developed an idealized microstructural representation of the a/d interface for micromechanical finite element analysis.[30,31] From the results of the analysis, we have shown that the mechanical property of the adhesive not only affects the overall bond or shear strength but also has a profound influence on the load transfer mechanism at the a/d interface and its fatigue life.[30–32] In addition, the change in the mechanical property of the adhesive with time can result in a gradual loss of the mechanical integrity of the a/d interface. The absorption of water by the adhesive polymer and leaching of unpolymerized monomer from the adhesive are linked to mechanical softening[20,33] and hydrolytic degradation.[3,34] The viscoplastic properties of the adhesive, in particular, change anomalously with water content under loading.[3,34–37] There is a concern that the effects of such liquid uptake and hydrolytic degradation may lead to a shortened service life for composite restorations.[38,39]

It is well known that the mechanical properties of cross-linked polymers and their interaction with solvents are strongly dependent on their chemical structure and composition.[40] Furthermore, we determined that hydrophilicity and cross-link density are two important independent variables, which affect the equilibrium water content (EWC) and diffusion rate into methacrylate-based cross-linked polymers.[41]

The different penetration of hydrophilic and hydrophobic monomers, coupled with phase separation, implies that the polymer phases in the a/d interface of the hybrid layer can range from viscoelastic glassy solids to soft elastomers under wet conditions. Our group has researched the polymerization kinetics and the network structure of hydrophilic-rich phases on the phase boundary of the ternary phase diagram.[42–45] Characterizing the chemomechanical properties of phases along the full length of the phase boundary on the basis of their composition will be useful for predicting the effect of water on the mechanical performance and durability of the composite restoration. To this end, the current study measures and correlates the following properties for the polymers on the phase boundary of the ternary phase diagram with their composition: EWC, swelling, nature of adsorbed water, equilibrium elastic modulus under wet and dry conditions, stress and strain at failure, storage modulus, loss tangent, and glass transition temperature.

II. MATERIALS AND METHODS

A. Materials

The "model" methacrylate-based dentin adhesive formulations were prepared as mixtures of HEMA, BisGMA, and deionized water. The monomers were purchased from Sigma Chemical Co., St. Louis, MO, USA. The chemical structures of the comonomers are shown in Table I. The following three-component visible light photoinitiators (all from Aldrich, Milwaukee, WI) were used in this work: camphorquinone (CQ, 0.5 wt. %), ethyl-4-(dimethylamino) benzoate (EDMAB, 0.5 wt. %), and diphenyliodonium hexafluorophosphate (DPIHP, 0.5 wt. %) without further purification. The concentration of the photoinitiator component is calculated with respect to the total amount of monomer. All materials were used as received.

B. Preparation of neat adhesive resins

Monomer mixtures in the following mass ratios of HEMA to BisGMA: (a) 95:5, (b) 92.5:7.5, (c) 80:20, (d) 75:25, (e) 70:30, (f) 60:40, (g) 45:55, (h) 30:70, and (i) 15:85 were added along with a three-component photoinitiator system (0.5 mass % of CQ, EDMAB, and DPIHP) into brown vials. The corresponding molar ratios of HEMA to BisGMA in the mixtures are (a) 99:1, (b) 98:2, (c) 94:6, (d) 92:8, (e) 90:10, (f) 86:14, (g) 76:24, (h) 63:37, and (i) 41:59. A balance with a resolution of 0.01 mg (Mettler Toledo, X205 dual range) was used to weigh each component and was used for all weight measurements described henceforth. The monomer–initiator mixtures were mixed thoroughly to give a homogeneous resin.

C. Determination of water miscibility of neat adhesive resins

About 1 g of each neat resin was weighed into a brown vial and water was added in increments of approximately 0.01 g until the mixture is visually observed to be turbid.

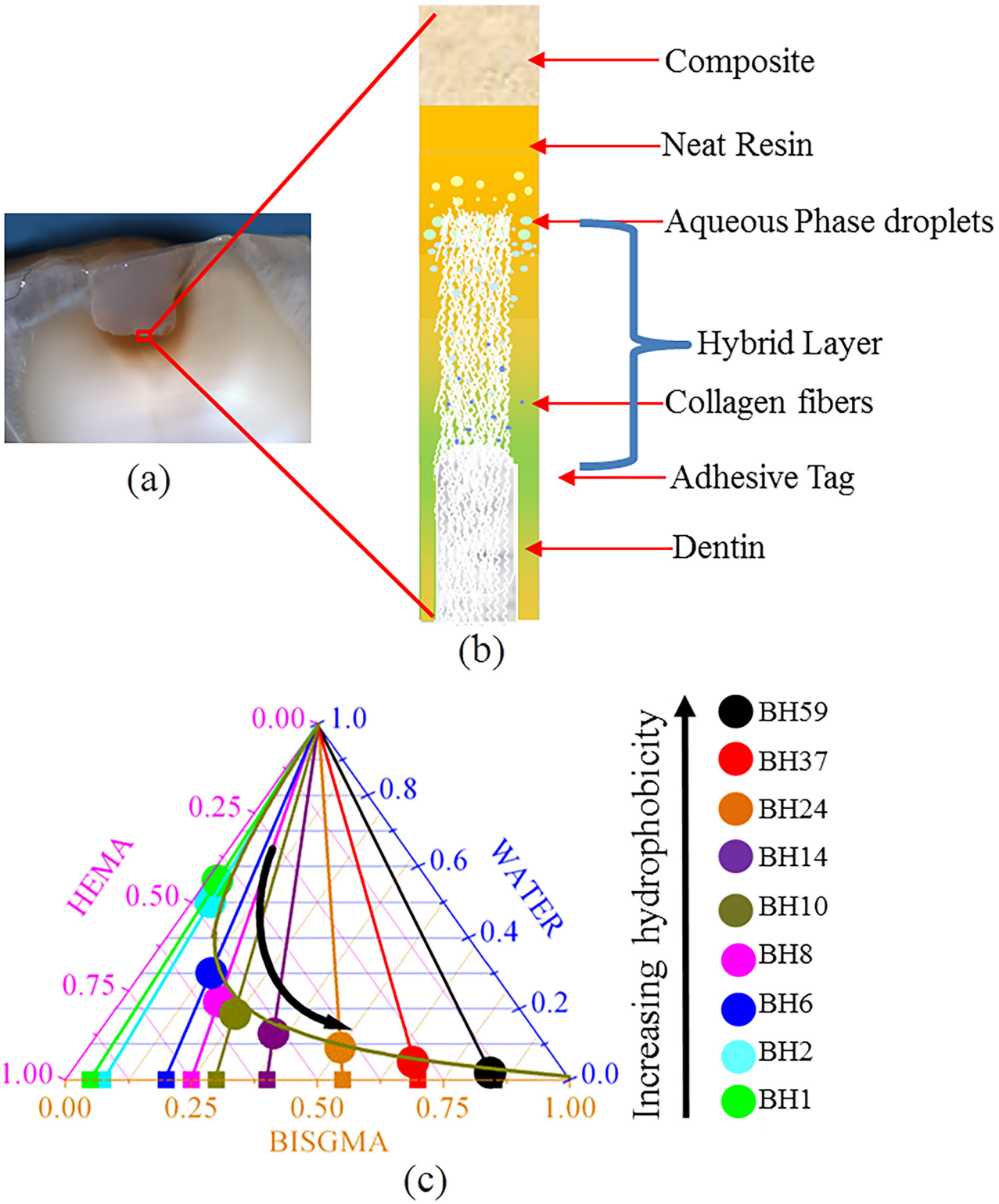

FIG. 1. (a) Exfoliated primary molar with class II composite restoration, (b) schematic of the dentin adhesive interface, and (c) representative adhesive monomer formulations identified on the phase boundary of the water-adhesive ternary phase diagram. The circles represent the formulations prepared close to the phase boundary. The squares represent the corresponding neat formulations.

The percentage of water in the mixture is noted (w_1). The mixture is then back-titrated using the neat resin until the turbidity disappears, and the percentage of water in the mixture is noted (w_2). The water miscibility is calculated as the average of w_1 and w_2. The procedure can be represented on the ternary phase diagram [Fig. 1(c)] as changing the water content along the line of constant monomer ratio starting at the neat resin (square point) on the BisGMA axis and

TABLE I. List of comonomers.

Comonomer chemical formula/name	Comonomer structure
BisGMA	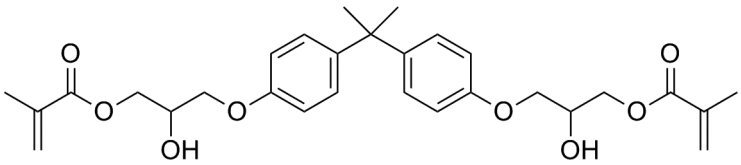
HEMA	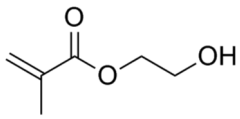

connecting to the water apex. The miscibility limit for the given monomer ratio is achieved where the line intersects the phase boundary.

D. Preparation of polymer samples from monomer–water formulations close to the phase boundary

Water equivalent to about 2%–3% below the miscibility limit is added to each neat resin and mixed till fully dissolved. In the absence of water, neat BisGMA and HEMA dissolve in a wide variety of concentration ratios and copolymerize to yield a copolymer which is uniform at the microscale.[46] In this study, the water content was chosen to lie within the miscibility limit to prevent the formation of any defects from polymerization induced phase separation at the scale of this study.[42] The composition of these formulations has been represented using circular points on the ternary phase diagram as shown in Fig. 1(c). The nomenclature BHX is used to represent the composition of these formulations where B represents BisGMA, H represents HEMA, and X is the mole percent of BisGMA in the neat resin before dilution. For example, BH14 is the formulation with a BisGMA mole fraction 0.14 in the neat resin before dilution, corresponding to the purple circle in Fig. 1(c). It is obtained by diluting the neat resin corresponding to the purple square in Fig. 1(c).

Square beams with a side of 1 mm and a length of at least 10 mm were prepared for each formulation by casting these prepared adhesive resins into glass tubing molds (Fiber Optic Center Inc., #CV1012, Vitrocom Round Capillary Tubing of Borosilicate Glass). The resins were injected into the tubing using a micropipette and polymerized in a LED light curing unit at intensity 250 mW/cm^2 for 40 s (LED Curebox, Prototech, Portland, OR). The effective irradiance was provided by the manufacturer based upon the intensity of the blue LED used in the box. The wavelength of light for the LED curebox is around 470 nm. The polymerized samples were stored in dark at room temperature for 2 days to provide adequate time for postcure polymerization. The samples were subsequently extracted from the glass tubing and stored in a vacuum oven in the presence of a drying agent (freshly dried silica gel) at 37 °C.

E. Degree of conversion

The degree of conversion (DC) was determined by Raman spectroscopy as described previously.[47] In brief, LabRAM ARAMIS Raman spectrometer (LabRAM HORIBA Jobin Yvon, Edison, New Jersey) was used with a HeNe laser ($\lambda = 633$ nm, a laser power of 17 mW) as an excitation source. The instrument settings were as follows: 200 μm confocal hole, 150 μm wide entrance slit, 600 g/mm grating, and 10× objective Olympus lens. Data processing was performed using LABSPEC 5 (HORIBA Jobin Yvon). The samples were mounted on a computer-controlled, high-precision x-y stage. To determine the DC, spectra of the unpolymerized resins and rectangular beam samples were acquired over a range of 700–1800 cm^{-1}. The changes of the band height ratios of the aliphatic C=C double bond peak at 1640 cm^{-1} to the aromatic C=C at 1610 cm^{-1} (phenyl) in both the cured and uncured states were monitored. Based on the decrease in the intensity of band ratios before and after light curing, the DC was calculated as follows:

$$\mathrm{DC}(\%) = \left[1 \frac{\mathrm{R}_{\mathrm{cured}}}{\mathrm{R}_{\mathrm{uncured}}}\right] \times 100, \quad (1)$$

where R = band height at 1640 cm^{-1}/band height at 1610 cm^{-1}. All experiments were carried out in triplicate over each sample area and across samples and the results were averaged.

F. Swelling experiment

Beam specimens are used to study the swelling behavior of each copolymer formulation. At least five samples were used for each formulation. Distilled, deionized water [high-performance liquid chromatography (HPLC) grade, W5SK-4, Fisher Scientific, Fair Lawn, NJ, USA] is used throughout the experiments. In order to extract the leachables, the beam specimens were first immersed in water till they attained constant mass. They were then placed into a vacuum chamber for drying until a constant mass was obtained. The specimens were weighed in air (m_{a0}) and weighed under distilled, deionized water (m_{w0}). The measurement under water is performed within about 10 s to avoid any absorption of water during the process. The

weight under water is equal to the weight in air minus the buoyancy force exerted by the water. The specimens were then immersed in water and stored at room temperature. At fixed time intervals (5, 10, 20, 40 min, 1, 2, 3, 5, 7, 10, 24, 36, 48, and 72 h), the specimens were retrieved, blotted dry to remove excess liquid, weighed in air (m_a), weighed in water (m_w), and returned to the liquid bath. If the specimens were not saturated, i.e., the specimens had not attained constant mass, the specimens were returned to the liquid bath and data were collected at additional intervals spaced 24 h apart until constant mass was reached. The volume of the sample was calculated using the weights in air and water as follows:

$$V = \alpha \frac{m_a - m_w}{\rho_w - \rho_a}, \tag{2}$$

where V is the volume of the sample, m_a is the weight of the sample in air, m_w is the weight of the sample in water, and $\alpha = 0.99985$ is a factor to account for air buoyancy. $\rho_w = 1$ g/cm^3 and $\rho_a = 0.0012$ g/cm^3 are the densities of water and air, respectively. The fractional mass change in air (Δm_a) and volume change expressed using the Jacobian of deformation, J, were calculated as follows:

$$\Delta m_a(\%) = \frac{m_a - m_{a0}}{m_{a0}}, \tag{3}$$

$$J = \frac{V}{V_0}. \tag{4}$$

G. Mechanical testing

Mechanical tests were performed using a three-point bending apparatus with 10 mm beam span on a Bose Electroforce 3200 tester. Loading was applied at a rate of 0.001 mm/s or equivalently in terms of the elastic strains at the rate of 60 microstrain/s. For the mechanical test in dry condition, the polymer beam samples were used as prepared. For wet testing, the samples were stored in water at 37 °C for at least 5 days and up to 15 days until the samples were completely saturated and no further change in mass was observed. Average stress–strain curves were obtained and used to calculate the elastic modulus from the linear region using at least three samples for each formulation under dry and wet conditions, respectively.

H. Dynamic mechanical analysis

The measurement of glass transition temperature (T_g) and apparent rubbery modulus was carried out using dynamic thermomechanical analysis (DMA Q800, TA Instruments, New Castle, USA) in a three-point bending configuration. The analysis has been described previously.[47] The frequency used to measure the storage modulus was 1 Hz with amplitude of 15 μm and a preload of 0.01N. The storage modulus was measured across 0–250 °C using a temperature sweep conducted at 3 °C/min. The T_g was identified from the peak of the loss tangent–temperature curve. The storage modulus decreased with temperature and registered an approximately linear increase beyond T_g; the value at T_g was taken to be the apparent rubbery modulus of the polymer.

I. Determination of cross-link density

Assuming that the adhesive polymers obey Flory's rubber elasticity theory[48] at temperatures slightly higher than T_g, the effective cross-link density, ν_e in moles/m^3, was calculated as follows:

$$V_e = \frac{E'}{3RT_g}, \tag{5}$$

where E' is the apparent rubbery modulus, T_g is the glass transition temperature of the polymer, and the universal gas constant $R = 8.31$ J K^{-1} mol^{-1}.

The stoichiometric cross-link density ν_s in moles/m^3 was calculated from the mole percentage of the cross-linker and the degree of conversion as follows:

$$\nu_s = \frac{100b(DC)\rho}{M_b}, \tag{6}$$

where b is the percentage of BisGMA in the polymer, DC is the percentage degree of conversion, ρ is the polymer density, and M_b is the molar mass of BisGMA. The degree of conversion was assumed to be uniform for BisGMA and HEMA segments; therefore, the stoichiometric cross-link density from Eq. (6) is an approximate estimate. The exact value will depend on the individual degree of conversion of BisGMA segments. The estimate from Eq. (6) provides a reasonable basis for comparison with effective cross-link density from Eq. (5).

J. Stoichiometric analysis

Stoichiometric analysis is used to calculate the percentage of hydrogen bonds between the OH groups for the following pairs of polymer segments: HEMA–HEMA, BisGMA–BisGMA, and BisGMA–HEMA. The following steps are used considering the example of a polymer phase formed from a neat resin containing BisGMA:HEMA in the mass ratio 85:15.

1. Total mass of the dry polymer = 100 g.
2. Mass of HEMA monomer segments, $m_{HEMA} = 15$ g, mass of BisGMA monomer segments, $m_{BisGMA} = 85$ g.
3. Molecular mass of HEMA, $M_{HEMA} = 130.14$, molecular mass of BisGMA, $M_{BisGMA} = 512.599$.
4. Number of moles of HEMA segments, $n_{HEMA} = m_{HEMA}/M_{HEMA} = 15/130.14 = 0.115$, number of moles of BisGMA segments, $n_{BisGMA} = m_{BisGMA}/M_{BisGMA} = 85/512.599 = 0.166$.
5. Number of moles of OH groups belonging to HEMA segments = $n_{HEMA} = 0.115$, number of moles of OH groups belonging to BisGMA segments = $2n_{BisGMA} = 0.332$.
6. Probability that the OH group on a polymer chain belongs to HEMA, $p_{OH,\ HEMA} = n_{HEMA}/$

$(n_{HEMA} + 2n_{BisGMA}) = 0.258$, probability that the OH group on a polymer chain belongs to BisGMA, $p_{OH,\ BisGMA} = 2n_{BisGMA}/(n_{HEMA} + 2n_{BisGMA}) = 0.742$. Therefore,

(a) Probability that the OH–OH hydrogen bond is between two HEMA segments, $p_{HEMA-HEMA} = p^2_{OH,\ HEM} = 0.0665$.

(b) Probability that the OH–OH hydrogen bond is between a HEMA segment and a BisGMA segment, $p_{HEMA-BisGMA} = p_{OH,\ HEMA} \times p_{OH,\ BisGMA} = 0.383$.

(c) Probability that the OH–OH hydrogen bond is between two BisGMA segments, $p_{BisGMA-BisGMA} = p^2_{OH,\ BisGMA} = 0.551$.

7. From step 6, 6.651%, 38.278%, and 55.071% of the OH–OH hydrogen bonds correspond to HEMA–HEMA interactions, HEMA–BisGMA interactions, and BisGMA–BisGMA interactions, respectively.

K. Investigation of hydrogen bonding using deuterium oxide

Using a plastic mold, thin film samples of approximately 25 μm thickness were cast using the neat adhesive resin monomers (Sec. II B). The BisGMA:HEMA ratios of the neat monomer mixtures were 40:60, 55:45, 70:30, 77.5:22.5, and 85:15. Mixture compositions with higher HEMA:BisGMA ratios were not considered because of the difficulty in handling thin film samples in the water saturated state.

Using a Perkin Elmer Spectrum 400 Fourier transform infrared spectrophotometer in transmission mode, FTIR spectra were collected for the thin film samples. In order to avoid spectral interference from water, deuterium oxide (D_2O; Cambridge Isotope Laboratories Inc., Andover, MA, USA) was used to investigate the effect of water absorption on the intermolecular and intramolecular hydrogen bonds in the polymer structure. Therefore, the thin films were soaked in a bath of D_2O to allow absorption until equilibrium saturation was achieved. FTIR spectra in transmission mode were collected for the D_2O-saturated thin films immediately after removal from the bath, to avoid loss of D_2O by evaporation. Example spectra for the polymer samples under dry and wet conditions along with the peaks used for analysis are shown in Fig. 2.

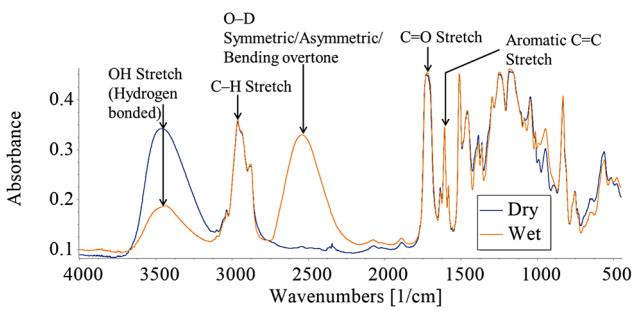

FIG. 2. FTIR spectra and characteristic peaks for a polymer phase from a BisGMA:HEMA = 85:15 neat resin in dry and wet conditions.

The ratio of the band area of the D_2O peak (~2175–2750 cm^{-1}) to the band area of the aromatic C=C peak (~1608 cm^{-1}), denoted as the D_2O/Ar ratio, was measured for each neat resin composition and used as an indicator of water absorption. The ratio of the band area of the OH peak (~3140–3725 cm^{-1}) to the aromatic C=C peak (~1608 cm^{-1}), denoted as the OH/Ar ratio, was used to study the vibration of the OH bond. This vibration could involve symmetric stretching mode, asymmetric stretching mode, as well as bending overtones. The change in this band ratio from the dry polymer film to the D_2O-saturated polymer film was used as an indicator of the disturbance to the OH vibration modes caused by the absorption of D_2O. All band areas were calculated using a linear baseline between the ends of each peak.

The OH peaks (~3140–3725 cm^{-1}) from the dry samples were fit using a single Bigaussian distribution for each peak. The OH peaks from the D_2O-saturated samples were fit using two Bigaussian curves due to the presence of a single shoulder. ORIGINPRO 2018 was used for the fitting procedures. The peaks of the fit curves were used to investigate the effect of D_2O absorption on the intermolecular and intramolecular hydrogen bonding.

III. RESULTS AND DISCUSSION

The phase boundary of the HEMA–BisGMA–water ternary system is shown in Fig. 1. HEMA is more soluble in water than BisGMA; therefore, the phase boundary extends from the hydrophilic end with almost no BisGMA and HEMA:water in the ratio 15:85 to the hydrophobic end with nearly pure BisGMA with no water. The negligible solubility of BisGMA in water is readily understood from the hydrophobic effect that would be generated by bulky aromatic groups and large nonpolar regions of the molecule.[49,50] The composition of a formulation lying on the phase boundary follows a well-defined curve and hence is fully defined by the percentage of one of the components. Since we use formulations close to but not exactly on the phase boundary, the resin composition follows an approximate curve.

A. Degree of conversion

The DC of all the polymerized phases along the phase boundary is shown in Fig. 3. The DC was found to be in the range 87% to nearly 100%. As the free radical polymerization proceeds, microgels of polymer with dissolved monomer and water form that are separated from the remaining monomer–water mixture. The increase in DC with water content can be attributed to the consequent decrease in viscosity of the sol-phase, which promotes diffusion of reactive species between the sol-phase and the microgel phase, resulting in a secondary polymerization regime.[42] In the case of the BisGMA-rich phases, further propagation of the polymerization reaction is limited by the diffusion rate of the reactive species from the monomer–water mixture into the

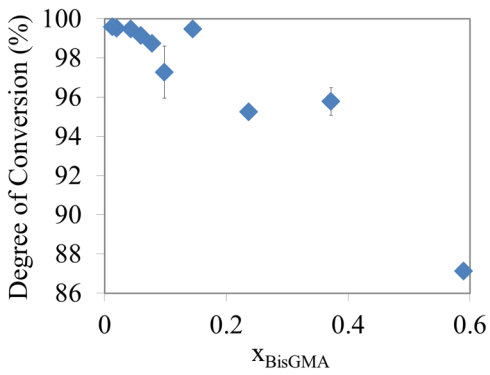

FIG. 3. Degree of conversion vs mole fraction of BisGMA for polymer phases along the phase boundary.

microgel, which depends on the viscosity of the resin.[43] A similar phenomenon has been observed for vinyl-ester microgels[51] and also as the cage effect for free radical polymerization.[52]

B. Cross-link density

Figure 4 shows both the effective cross-link density ν_e, calculated using Eq. (5), and the stoichiometric cross-link density ν_s, calculated using Eq. (6). Both the effective and stoichiometric cross-link density increase with BisGMA, but we observe that the stoichiometric prediction based on the degree of conversion is close to the values predicted from the rubbery modulus for BisGMA mole fraction up to about 0.14, showing that the material can be described by the statistical theory of rubbery elasticity.[48] For higher mole fractions of BisGMA, the effective cross-link density is much higher than the stoichiometric cross-link density. The likely reasons for this difference are (i) the inadequacy of the affine rubbery elasticity as the chain length decreases with increase in BisGMA content [see Chapter 1 (Ref. 53)], (ii) energetic contributions of the noncovalent interactions which are still mechanically active in resisting interatomic bending and shear[54] at temperatures beyond T_g, as well as (iii) the decrease in free volume for chain motion due to large size of BisGMA segments. Since the stoichiometric cross-link density calculation is approximate, so is the BisGMA mole fraction at which the effective cross-link density departs from the stoichiometric cross-link density. The results nevertheless show the dramatic nonlinear departure from elastomeric behavior with increasing mole fraction of BisGMA.

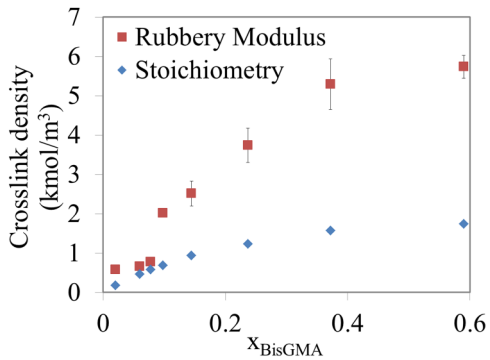

FIG. 4. Cross-link density obtained from rubbery modulus and stoichiometry for polymer phases along the phase boundary.

C. Equilibrium water content and equilibrium swelling

Figures 5(a) and 5(b) show the variation in EWC and equilibrium swelling with BisGMA content. We observe that the EWC and swelling decrease with BisGMA content. The EWC values range from more than 70% in the most hydrophilic polymer (7.5% BisGMA) to about 3.4% in the most hydrophobic polymer (85% BisGMA). The increased covalent cross-link density of the polymer with BisGMA as well as the decrease in hydrophilicity with BisGMA content are responsible for the reduction in swelling and EWC. The reduction in EWC for methacrylate-based polymers with increased cross-link density and decreased hydrophilicity has been shown earlier.[41] We note that the EWC drops rapidly with BisGMA till a mole fraction of about 0.1 and then drops at a slower rate. The nature of change in free energy of the polymer upon water sorption resulting from mixing entropy and enthalpy changes, and pore fluid pressure depends on the covalent cross-link density, noncovalent interactions between polymer chain segments, as well as hydrophilicity, and contributes to this nonlinear decrease of EWC with an increase in BisGMA content.[55] Increased nonlinearity in EWC with respect to cross-linker content has been observed for HEMA-based copolymers when the cross-linker also happens to be hydrophobic and has been attributed to the combined effect of hydrophobicity and cross-linking.[56] The leachables extracted after swelling primarily

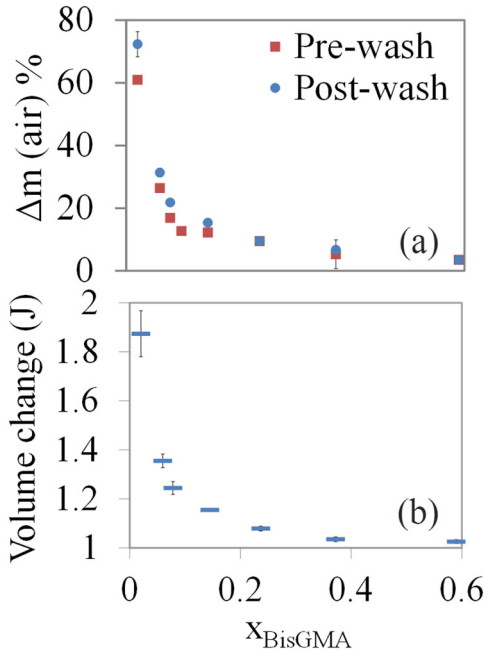

FIG. 5. Variation of (a) equilibrium water content, and (b) Jacobian of equilibrium swelling with mole fraction of BisGMA, for polymer phases along the phase boundary.

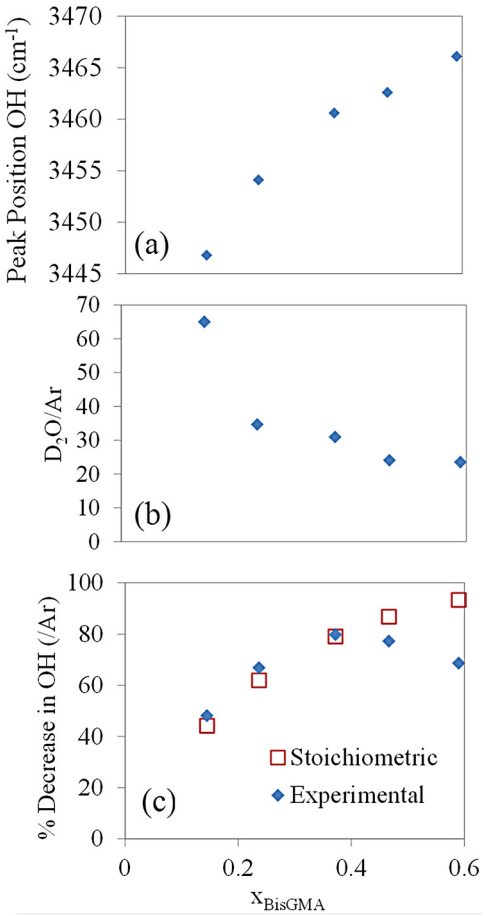

FIG. 6. Variation in peak position of the OH peak in the dry polymer formulations, (b) variation of the band area ratio of D_2O band to the aromatic C=C, plotted against mole fraction of BisGMA in the polymer, for polymer phases formed from neat resins.

consist of unpolymerized monomers HEMA and BisGMA, and coinitiators. An inverse correlation between monomer release and degree of conversion has been shown in earlier work.[57] The kinetics of leaching has also been analyzed directly using HPLC (Refs. 57 and 58) and indirectly using mass change experiments.[41]

D. Molecular investigation from FTIR spectra

Figure 6(a) shows the variation of the OH peak position in the dry polymer. The peak positions show an increasing trend with BisGMA mole fraction, indicating increasingly stiffer hydrogen bonding of the OH group. Figure 6(b) shows the decrease in the D_2O/Ar ratio with mole fraction of BisGMA. As expected, the trend shown by the data is similar to the variation of EWC with BisGMA mole fraction shown in Fig. 5(a). The two trends are not identical; these differences are attributable to sample composition, i.e., the experiments described in Sec. II K are performed using neat resin samples, while the mass change experiments (water sorption and swelling—described in Sec. II F) are performed using samples close to the phase boundary.

Figure 6(c) shows the percentage decrease in the OH/Ar ratio plotted against the mole fraction of BisGMA, from both experimental observation and stoichiometric calculation. Table II shows the corresponding numerical values. The stoichiometric calculation is performed as per the procedure described in Sec. II J assuming that only the OH–OH hydrogen bonds from BisGMA–BisGMA interactions and HEMA–BisGMA interactions undergo H–D exchange with D_2O. Correspondingly, the sum of $p_{HEMA–BisGMA}$ and $p_{BisGMA–BisGMA}$, shown in Table II, gives the theoretically expected percentage change in the OH/Ar ratio. The experimentally observed percentage change initially increases, reaches a maximum at a BisGMA mole fraction of 0.37 (BH37), and then decreases. We hypothesize that the decrease in the OH/Ar ratio is due to the exchange of the hydrogen atom of the OH group with the deuterium atom in D_2O. This exchange is indicative of the nature and extent of hydrogen bonding between the OH group of the polymer and the D_2O molecule. The differences between the theoretically expected decrease and the experimentally observed decrease are discussed below.

Water in hydrophilic polymers has been classified as strongly bound (nonfreezing), weakly bound (intermediate), or nonbound (freezing) based on the characteristic temperatures of phase transition.[59,60] Literature on methacrylate-based cross-linked hydrogels shows a complex nonlinear dependence of the nature of water on cross-linker content and hydrophobicity.[56,61] In general, it has been observed using several experimental techniques, including thermal expansion and differential scanning calorimetry, that high-water content hydrogels tend to have an increased content of nonbound (freezing) water.[62]

With these considerations, we propose that the most likely reason for the observed trend is because at higher D_2O concentrations (lower mole fraction of BisGMA), the D_2O exists in a state closer to nonbound or freezing water, preferentially forming hydrogen bonds with other D_2O molecules rather than with the OH functional group on HEMA

TABLE II. Probabilities for OH–OH hydrogen bonding within the polymer phases.

Formulation	x_{BisGMA}	$p_{HEMA–HEMA}$	$p_{HEMA–BisGMA}$	$p_{BisGMA–BisGMA}$	$(p_{HEMA–BisGMA} + p_{BisGMA–BisGMA})100$	% decrease in OH/Ar ratio
BH59	0.59	0.067	0.38	0.55	93	69
BH47	0.47	0.13	0.46	0.40	87	77
BH37	0.37	0.21	0.50	0.30	79	80
BH24	0.24	0.38	0.47	0.15	62	67
BH14	0.14	0.56	0.38	0.064	44	48

TABLE III. Peak positions for OH peaks in wet and dry conditions and for the D_2O peak in wet condition.

		Dry condition	Saturated with D_2O			
Neat resin composition	x_{BisGMA}	OH peak position	OH peak position (low wavenumber)	OH peak position (high wavenumber)	Average peak position of OH	D_2O peak position
BH59	0.59	3466.1	3364.65	3517.34	3441.00	2541
BH47	0.47	3462.6	3366.86	3518.41	3442.64	2534
BH37	0.37	3460.6	3366.80	3513.21	3440.00	2537
BH24	0.24	3454.1	3367.64	3520.78	3444.21	2536
BH14	0.14	3446.8	3355.93	3486.73	3421.33	2514

and BisGMA segments, leading to reduced deuterium exchange with the OH functional groups. Conversely, for lower D_2O concentrations (higher mole fraction of BisGMA), the D_2O strongly interacts with the OH functional groups of the polymer, leading to larger deuterium exchange. Such observations have also been reported for the water absorption into cross-linked hydrophilic polymer networks using molecular dynamics simulation.[63–66] We attribute the decreasing trend at higher BisGMA mole fractions to decreasing availability of OH binding sites due to increased steric occlusion, as has been proposed earlier for other cross-linked copolymer systems containing HEMA.[56] A similar trend for freezable bound water with hydrophobic comonomer content has been observed for methyl methacrylate *N*-vinyl 2-pyrrolidone xerogels cross-linked with ethylene glycol dimethacrylate.[67]

The stoichiometric calculations using the procedure outlined in Sec. II J and shown in Table II closely predict the observed trends for BH14, BH24, and BH37, strongly suggesting that the OH groups which are part of BisGMA–BisGMA interactions or BisGMA–HEMA interactions have stronger interactions with the D_2O molecules, leading to H–D exchange and consequent drop in the OH/Ar band ratio. The effect of steric occlusion due to BisGMA causing decreased availability of OH sites to bond with D_2O is prominent in BH47 and BH59.

Further evidence of the nature of hydrogen bonding in the wet polymer is also observed from the peak position of the D_2O peak in the D_2O-saturated samples. Table III shows the peak positions for the D_2O peak. The D_2O peak positions for BH59, BH47, BH37, and BH24 are dropping very gradually while the peak position for BH14 is significantly different at 2514 cm^{-1}. Noting that the spectral peak position for pure D_2O is 2504 cm^{-1}, we observe that the D_2O peak for BH14 has moved closer to the pure D_2O peak, indicating that the D_2O in BH14 is closer to free water, as compared to the rest of the polymer phases. Similarly, we note from Figs. 5(a) and 5(b) that the steep rise in EWC and in equilibrium swelling begins close to BH14.

E. Elastic moduli in wet and dry conditions

Figure 7 shows a comparison of the elastic moduli of the polymers in dry, wet, and rubbery elastic conditions. The elastic moduli under dry and wet conditions are measured at room temperature (25 °C), while the rubbery modulus is measured at a temperature slightly higher than T_g in the rubbery region. The elastic moduli in both dry and wet conditions show an increasing trend with the mole fraction of BisGMA in the monomer formulation. The rubbery modulus also increases with BisGMA content but does not follow the statistical theory of rubbery elasticity, as explained in Sec. III B. For BH2, the rubbery modulus is higher than

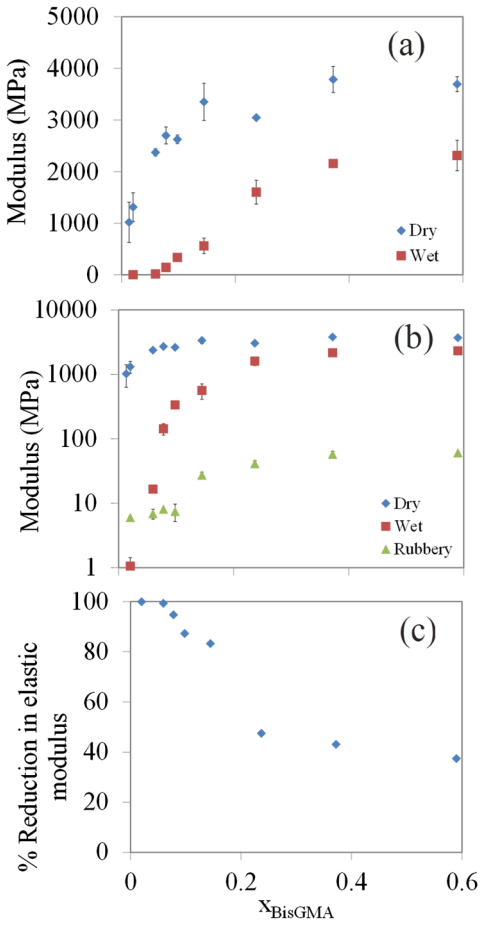

FIG. 7. Elastic moduli in dry and wet conditions at 25 °C and rubbery modulus vs the BisGMA mole fraction in the corresponding neat monomer formulation plotted on (a) linear scale, (b) semilog scale, and (c) percentage reduction in elastic modulus under wet conditions, for polymer phases along the phase boundary.

the wet modulus. For BH6, we observe that the rubbery modulus is close to the wet modulus; beyond this value, the elastic modulus in the wet condition follows a different slope with BisGMA content.

Figures 7(a) and 7(b) show the variation in the elastic moduli of the polymer phases with increasing mole fraction of BisGMA. In the dry condition, the covalent cross-links between the polymer chains and the intrasegmental and intersegmental hydrogen bonding between polymer chains are important factors governing the overall mechanical stiffness at the molecular scale. The covalent cross-link density as well as the hydrogen bond stiffness and density increase with BisGMA mole fraction leading to increased elastic modulus. The variation in the elastic moduli with mole fraction of BisGMA in the dry condition follows a logarithmic trend, unlike either the Voigt or Reuss estimate obtained solely based on the fraction of covalent bonds. Such a trend has also been observed for other cross-linked polymers.[68] Figure 7(b) also shows the variation in the rubbery modulus. Beyond the glass transition temperature, it is highly likely that chain segments between cross-links have almost all degrees of freedom set free with negligible viscous resistance, and the material tends toward an elastomer. The orders of magnitude difference between the rubbery moduli and the wet and dry moduli highlight the contribution of existing noncovalent interactions in the wet condition toward the polymer stiffness.

Figure 7(c) shows the percentage reduction in the modulus under wet conditions, which is observed to follow a sigmoid variation. The percentage reduction follows a certain slope through (BH59, BH37, and BH24); below the BisGMA mole fraction of 0.2, there is a dramatic increase in the percentage reduction of the elastic modulus. We explain this trend in the following manner: the reduction in elastic modulus in the wet condition is because the hydrogen bonding between the polymer chains is disturbed by water molecules. However, it has been pointed out that bound water, unlike free water, is capable of carrying shear stress.[69] Therefore, the reduction in elastic modulus under wet condition is attributed to two reasons: (i) the reduction in intersegmental shear stiffness between polymer chains which interact via bound water bridges in the wet condition as opposed to interacting directly as in the dry condition and (ii) due to the free water clusters in the interstices between polymer chains. Free water prevents the hydrogen bonding between the polymer chains and itself does not transmit shear stress.

Based on the stoichiometric comparison in Fig. 6(c), we conclude that phenomenon (i) occurs primarily for water that disturbs hydrogen bonds in HEMA–BisGMA or BisGMA–BisGMA interactions, while phenomenon (ii) occurs primarily for water that disturbs hydrogen bonds in HEMA–HEMA interactions. From Figs. 5(a), 5(b), and 6(b), we can infer that there is a dramatic increase in the free water content from BH14 onwards toward the hydrophilic end of the phase boundary. The percentage reduction of modulus shows a much steeper increase from BH14 onwards. In BH6 and BH2, a large majority of the hydrogen bonds are expected to be part of HEMA–HEMA interactions because these two phases lose almost 100% of their stiffness in wet conditions and become pure elastomers. On the hydrophobic side, it is clear that for BH59, BH37, and BH24, the decrease in elastic modulus is predominantly due to bound water, and the percentage reduction shows a much shallower slope.

As the BisGMA mole fraction increases, the polymer approaches a network structure due to high covalent cross-link density. Furthermore, the lower mechanical compliance associated with aromatic groups[70] also increases the stiffness with BisGMA under both wet and dry conditions. The increased content of free water clusters in hydrophilic-rich phases indicates that a conventional poroelastic model in which the pore water responds to the pore volume change may be used to describe these phases. On the other hand, a more general chemo-micro-poromechanical constitutive law involving a more sophisticated energetic description including the decomposition between pore volume change and polymer–water interaction[71] is necessary to describe the mechanical behavior of the wet hydrophobic-rich phases.

F. Yield behavior in wet and dry conditions

Figures 8(a) and 8(b) show the apparent stress strain behavior in both dry and wet conditions of the polymer formulations along the water-adhesive phase boundary.

Figures 8(c) and 8(d) give the apparent failure strain with the mole fraction of BisGMA under dry and wet conditions, and Fig. 8(e) shows the variation in loss tangent with temperature for the different polymer phases. We observe from Fig. 8(a) that in both the dry and wet conditions, the yield stress increases with BisGMA mole fraction. The polymers with an intermediate quantity of BisGMA show ductile behavior with significant plastic deformations while the polymers with either very low or very high percentage of BisGMA exhibit relatively brittle failure. As seen from Fig. 8(c), the apparent failure strain in the dry condition increases, peaks, and then falls with increase in BisGMA content. The increase in yield stress with BisGMA content can be attributed to the increase in the density of hydrogen bonds, increase in the density of covalent cross-links, and the introduction of aromatic groups. These changes increase the activation energy required for yielding and decrease the free volume, which increases the yield stress according to Eyring's first theory.[72,73] Under dry conditions, the adhesive polymer formulations are glassy polymers at room temperature and may fail by any of the following mechanisms: bond breaking, which is typically associated with brittle failure, and micro-shear band formation, which is typically associated with ductile failure and takes place by a viscous flow process.[74,75]

It has been experimentally demonstrated that the molecular motions involved in the yielding process are the same as those involved in the glass transition.[76] We obtain the information on the transition processes from the loss tangent data shown in Fig. 8(e). The polymer undergoes two transitions: a secondary

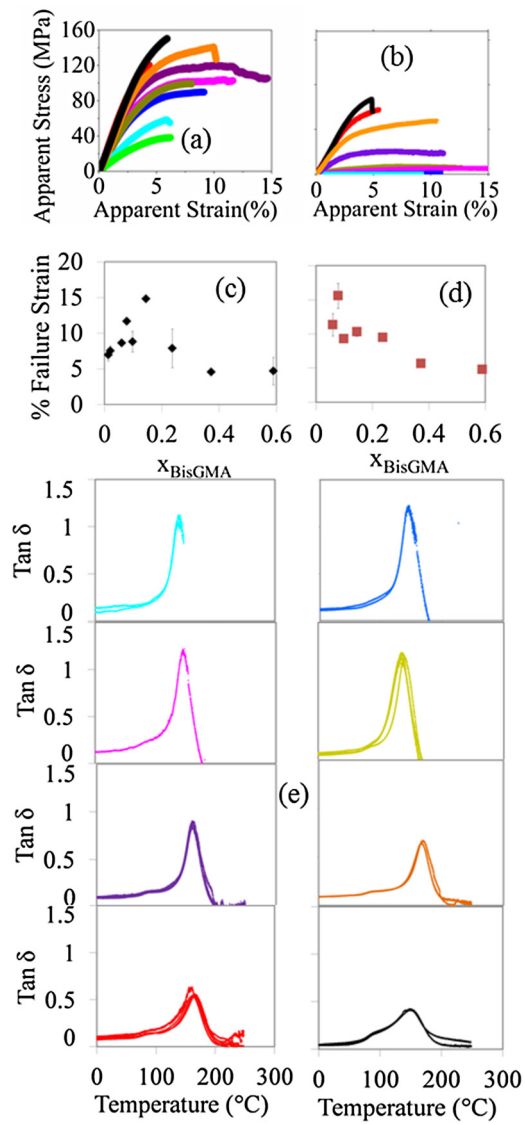

FIG. 8. Apparent stress strain behavior in (a) dry and (b) wet conditions at 25 °C, apparent failure strain in (c) dry and (d) wet conditions, and (e) loss tangent over temperature sweep for the polymer phases along the phase boundary.

transition appears first as a shoulder in the loss tangent graph at about 80 °C and the primary glass transition appears next at a much higher temperature around 160 °C. Following the terminology used by Roetling,[77,78] we assign the primary glass transition to correspond to an α-process and the secondary shoulder to a β-process. Two transitions have also been observed using differential scanning calorimetry for the polymer phases BH1 prepared using varying concentrations of D_2O (Ref. 42) and BH24 prepared using varying concentrations of ethanol.[79] Both the α-process and the β-process could be activated during yielding; however, the β-process is more likely since its characteristic temperature is closer to room temperature. From Fig. 8(e), we observe that the shoulder corresponding to the β-process becomes more significant with increasing BisGMA content. At low BisGMA content, where the shoulder associated with the β-process is negligible, the failure is brittle since the characteristic temperature of the α-process is much higher than room temperature. The contribution from the β-process increases with BisGMA content and increases the strain at failure until BH14. The β-process, being very close to room temperature, has a significant contribution to viscous flow at yield, thus increasing the yield strain. For phases more hydrophobic than BH14, the effect of the decrease in the available free volume for molecular motion becomes greater, discouraging viscous flow at failure. Furthermore, the increase in the density of intermolecular hydrogen bonds encourages brittle failure, decreasing the failure strain. Finally, for very high BisGMA content, the scope for viscous flow is reduced due to small free volume and high covalent cross-link density;[73] hence, the mode of failure is brittle.

Figure 8(b) shows that the yield stress in the wet condition is significantly smaller than in the dry condition. As discussed in Sec. III E, in the wet state, (i) the hydrogen bonds resulting from HEMA–HEMA interactions are no longer active, (ii) there is free water between the polymer chains, and (iii) there is bound water bridging between HEMA–BisGMA and BisGMA–BisGMA interactions. All of these factors contribute to the decrease in yield stress under wet condition. Figure 8(b) also shows that the polymer phases BH1, BH2, BH6, BH8, and BH10 transform into rubbery elastomers by orders of magnitude softer than BH14, BH24, BH37, and BH59. The dramatic increase in free water content from BH10 onwards is most likely responsible for this change in behavior. At intermediate (BH24 and BH14) and high (BH37 and BH59) BisGMA content, it is highly likely that the viscous flow phenomenon arising from the β-process is still present, resulting in similar failure strains as in the dry condition.

G. Viscoelastic properties

Figure 9 shows the viscoelastic properties of the polymer formulations at a frequency of 1 Hz and temperature of 25 °C for a maximum displacement magnitude of 15 μm or 900 microstrain. From Fig. 9(a), we observe that the storage modulus increases rapidly from BH1 to BH6 and then stays nearly constant. As expected, the trend for the storage moduli is similar to that of the elastic moduli shown in Fig. 7(a). The storage modulus increases as the density of hydrogen bonds, associated with the α-process, as well as the density of covalent bonds increase with BisGMA content. The degrees of freedom associated with the α-process do not transition into viscous flow at room temperature since the required activation energy is too high. They are restricted and contribute to elastic recovery under applied stress. The storage moduli are slightly larger than the elastic moduli and this difference is likely due to the fact that the storage moduli were measured at a frequency of 1 Hz and amplitude 15 μm, i.e., at a mean loading rate of 9.6 μm/s, which is 9.6 times faster than the 1 μm/s loading rate used to obtain the elastic moduli from three-point bending. At higher rate of loading, the polymer chains are less mobile and contribute more to the storage modulus.[40]

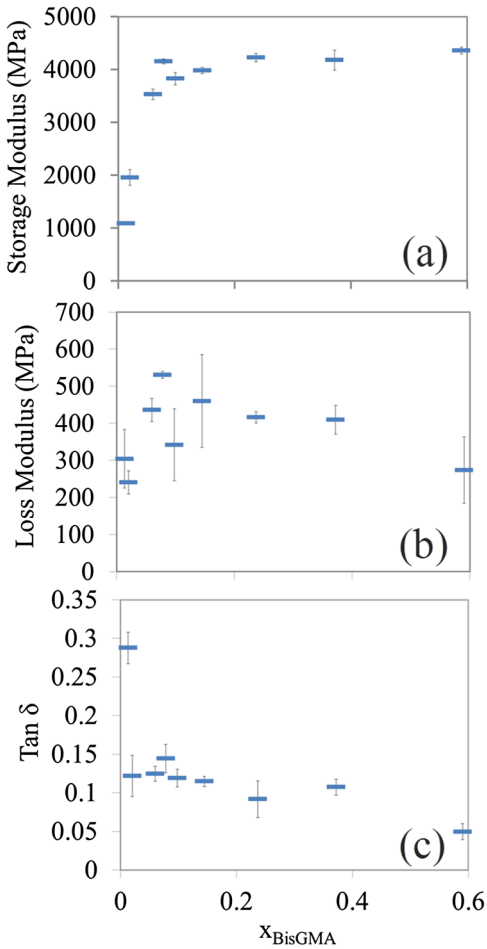

FIG. 9. Variation in viscoelastic properties of the polymer phases along the phase boundary with respect to BisGMA mole fraction measured at a frequency of 1 Hz, temperature of 25 °C, and displacement amplitude of 15 mm.

Figure 9(b) shows that the loss modulus goes through a peak and then decreases with BisGMA content. The variation of apparent failure strain with BisGMA content is similar to the variation of loss modulus with BisGMA [see Fig. 8(c)]. The loss modulus also represents the extent of energy absorbed by viscous flow; thus it is correlated to the extent of ductile failure. The loss modulus depends on the mobility of polymer chains and the frictional resistance to rearrangement of polymer chains under applied stress or strain. The initial increase in the loss modulus up to about 0.14 mole fraction BisGMA is due to increased contribution from the β-process and reflects increasing viscous resistance when sufficient mobility is available for those degrees of freedom. The decrease in loss modulus beyond about 0.14 mole fraction BisGMA is because the chains become largely immobilized with the increase in covalent cross-linking, which is also reflected in the increasing elastic modulus [see Fig. 7(a)].

The viscous flows contributing to ductility and viscoelasticity are both associated with the β transition. The loss tangent, tan δ, given by the ratio of the loss to storage modulus decreases with BisGMA content as shown in Fig. 9(c).

Since the loss tangent depends on the ratio of the viscous and elastic energies, it decreases monotonically due to the steady increase in the storage modulus. The steep drop in loss tangent from BH1 to the remaining formulations is likely due to the steep increase in interaction density and steric effects in this neighborhood. When the BisGMA concentration is very low, the distance between the BisGMA polymer segments is very large and the intersegmental hydrogen bonding is very weak. The decrease in the loss tangent with BisGMA concentration could be attributed to the following reasons: (a) decrease in the available free volume due to steric effects from the large size of BisGMA segments and (b) increase in noncovalent and covalent interactions with increasing BisGMA, particularly since it has been observed that the strength of the hydrogen bond falls off with the square of the distance between the molecules.[80] It is likely that the steep increase in storage modulus [see Fig. 9(a)] from BH1 onwards is also due to the same reason.

The T_g corresponding to the α-process, shown in Fig. 10(a), increases with percentage BisGMA and goes through a maximum before decreasing. The glass transition occurs at the temperature when a majority of the polymer chains have the maximum free volume and mobility while the material is still viscoelastic. The glass transition has been attributed most frequently to a loss of connectivity and increase of free volume as the intersegmental bonds in the polymer are no longer "long-lived" and mechanically active, and the characteristic time of reptation of the polymer chain falls by orders of magnitude.[54] This phenomenon is expected to happen as the noncovalent interactions among the polymer chains undergo a "melting transition" according to the Lindemann criterion.[81–84] The T_g is

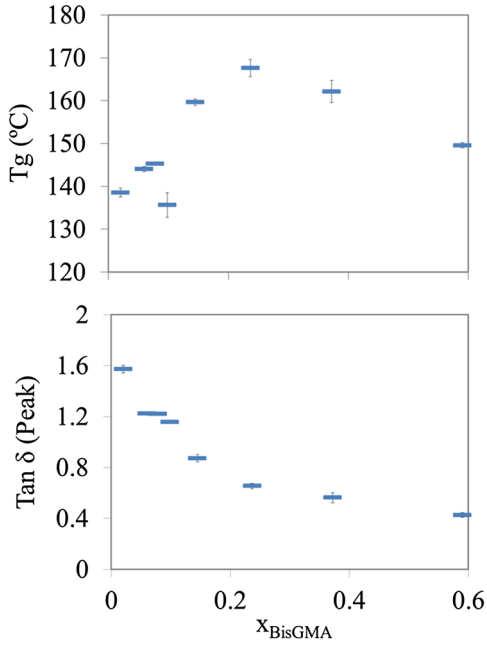

FIG. 10. Variation in (a) glass transition temperature and (b) peak loss tangent with mole fraction of BisGMA in the polymer phases along the phase boundary.

determined by the activation energy necessary to overcome the resistance to the degree of freedom associated with the α-transition. Initially, as BisGMA content increases, the activation energy for the α-transition increases due to increase in noncovalent bonding from hydrophobic effects, leading to an increase in T_g. However, with further increase in BisGMA content, a larger fraction of the polymer becomes bound together by covalent cross-links and the chain length of the mobile portions decreases. Thereby, the percentage of interactions involved in the α-transition decreases, leading to a decrease in the average activation energy and thereby the T_g. Therefore, the polymer becomes rubbery at a smaller temperature but with a higher rubbery modulus [as shown in Fig. 7(b)]. The decrease in proportion of mobile chains is also reflected in the decrease in peak loss tangent shown in Fig. 10(b).

IV. SUMMARY AND CONCLUSIONS

The chemomechanical behavior of polymers formed in the hybrid layer of a composite restoration has been studied using the polymer phases formed along the phase boundary of a water-adhesive ternary phase diagram. Static and dynamic mechanical properties as well as swelling have been explained on the basis of intermolecular interactions, polymer–water interaction, and the activation of viscous flow processes. We have also presented an experimental approach using FTIR spectroscopy along with accompanying stoichiometric calculations to evaluate the nature of interaction between adsorbed water and polymer segments. In summary, we have shown that

(i) The equilibrium water content follows a nonlinear variation along the phase boundary. Toward the hydrophilic end of the phase boundary, a majority of the water content is similar to free water, whereas a majority of the water content tends toward being bound as we approach the hydrophobic end of the phase boundary. We have discerned this based on the reduction in OH peaks in the FTIR spectra of D_2O-saturated polymer phases caused by H–D exchange.

(ii) The reduction in elastic modulus under wet conditions follows a sigmoidal trend along the phase boundary, which is strongly related to the nature and amount of water adsorbed by the polymer. Particularly, we attribute the steep decrease from BH14 onwards to the transition in adsorbed water from a bound state to free water clusters.

(iii) There are two separate characteristic transitions associated with the polymer phases: a primary α-transition and a secondary β-transition. Using the Ree-Eyring theory, these processes have been used qualitatively to explain the observed parallels between yield behavior and loss tangents along the phase boundary of the water-adhesive ternary phase diagram.

(iv) Both the glass transition temperature and loss modulus have a peak value on the phase boundary, indicating an interplay between several factors, including chain mobility and available free volume, viscous resistance to chain motion provided by noncovalent interactions, chain length between cross-links, as well as the density of interactions.

A crucial function of the dentin adhesive is to entrap the demineralized collagen so it is protected from enzymes, acids, and bacteria in the saliva. The transport of these species through the adhesive polymer is related to the connectivity of micropores in the adhesive, as well as the nature of water in the adhesive. Particularly, the availability of free water in the adhesive polymer facilitates the transport of solutes and species into the underlying tooth structure.[85] Furthermore, the activity of proteins and enzymes depends upon their association with water, and in turn, with the nature of the adsorbed water in the adhesive.[67,86,87] In this respect, it is important to ensure that the free water containing hydrophilic-rich polymer phases are not accessible to acids, enzymes, and bacteria in the mouth.

The properties obtained in this work can be used to further enhance the finite element models previously developed for the dentin/adhesive (d/a) interface.[30–32] We also see from the results presented in this paper that the variation in adhesive properties along the depth of the hybrid layer is nonlinear and nonmonotonic even if the composition varies monotonically. From the perspective of mechanical modeling, we note that under wet conditions, the polymer phases at the hydrophobic end are best described by a viscoelastic constitutive law, whereas those at the hydrophilic end are elastomers described by hyperelastic constitutive models. The phases in between require sophisticated poromechanical models which account for the nature of polymer–water interaction. This observation also motivates the development of micro-, meso-, or molecular-structure based constitutive laws which can reproduce such transitions in material behavior through smoothly varying model parameters. Such laws would be useful for modeling not only the d/a interface but also a number of biological interfaces linking materials which are mechanically dissimilar.[88–90]

In this context, we note that the investigation of molecular mechanisms behind mechanosorptive effects in materials[91] including dentin adhesives,[92] wood,[93] paper,[94] aramid fibers,[95] and other polymers and fiber-reinforced materials has been a research problem of considerable interest. We believe that the experimental procedure described in Sec. II K along with a stoichiometric analysis such as described in Sec. II J could be used as a basis to design experiments which could improve the understanding of the mechanisms behind this important phenomenon. In particular, the anomalous creep of dentin adhesives has been demonstrated in earlier work.[92] In our future work, we plan to implement the experimental technique presented in Sec. II K in real-time during mechanical testing to investigate the molecular scale mechanism behind this important phenomenon. These results can be used to inform the design of adhesives that are resistant to anomalous creep. Some of the experimental data in this paper have been used to develop

microporomechanical models to describe the swollen equilibrated state of polymer phases.[55,96,97] Further experimental results could be used to extend these models to describe failure under wet and dry conditions. The information could also be used to inform the rational design of dentin adhesives as one aspect of a multifaceted research strategy to improve mechanical behavior in wet conditions while maintaining or improving the monomer solubility and phase separation behavior.

ACKNOWLEDGMENTS

This investigation was supported by Research Grant Nos. R01DE022054 (PI: Spencer) and R01DE025476 (Spencer/Tamerler) from the National Institute of Dental and Craniofacial Research, National Institutes of Health, Bethesda. We also thank Lizhi Ouyang for discussion regarding deuterium exchange in D_2O-saturated polymers.

[1]L. Tjäderhane *et al.*, Dent. Mater. **29**, 999 (2013).
[2]M. Hashimoto, H. Ohno, H. Sano, F. R. Tay, M. Kaga, Y. Kudou, H. Oguchi, Y. Araki, and M. Kubota, J. Biomed. Mater. Res. **63**, 306 (2002).
[3]M. Hashimoto, H. Ohno, M. Kaga, K. Endo, H. Sano, and H. Oguchi, J. Dent. Res. **79**, 1385 (2000).
[4]H. Sano, T. Yoshikawa, P. N. R. Pereira, N. Kanemura, M. Morigamui, J. Tagami, and D. H. Pashley, J. Dent. Res. **78**, 906 (1999).
[5]P. Spencer and J. R. Swafford, Quintessence Int. **30**, 501 (1999).
[6]P. Spencer, Y. Wang, B. Bohaty, and J. Biomed, Mater. Res. Part B Appl. Biomater. **77**, 234 (2006).
[7]Y. Wang and P. Spencer, J. Dent. Res. **82**, 141 (2003).
[8]E. L. Kostoryz, K. Dharmala, Q. Ye, Y. Wang, J. Huber, J. G. Park, G. Snider, J. L. Katz, and P. Spencer, J. Biomed. Mater. Res. Part B Appl. Biomater. **88**, 394 (2009).
[9]P. Spencer *et al.*, Ann. Biomed. Eng. **38**, 1989 (2010).
[10]J. L. Ferracane, J. Dent. Res. **96**, 364 (2017).
[11]P. Spencer, Q. Ye, A. Misra, S.E. de P. Goncalves, and J. S. Laurence, J. Dent. Res. **93**, 1243 (2014).
[12]I. Nedeljkovic, J. De Munck, V. Slomka, B. Van Meerbeek, W. Teughels, and K. L. Van Landuyt, J. Dent. Res. **95**, 875 (2016).
[13]I. Nedeljkovic, W. Teughels, J. De Munck, B. Van Meerbeek, and K. L. Van Landuyt, Dent. Mater. **31**, e247 (2015).
[14]K. F. Leinfelder, J. Am. Dent. Assoc. **131**, 1186 (2000).
[15]R. Z. Thomas, H. C. Van Der Mei, M. H. Van Der Veen, J. J. De Soet, and M. Huysmans, Oral Microbiol. Immunol. **23**, 7 (2008).
[16]R. L. Bowen and W. A. Marjenhoff, Adv. Dent. Res. **6**, 44 (1992).
[17]P. A. Da Rosa Rodolpho, T. A. Donassollo, M. S. Cenci, A. D. Loguercio, R. R. Moraes, E. M. Bronkhorst, N. J. M. Opdam, and F. F. Demarco, Dent. Mater. **27**, 955 (2011).
[18]K. J. Anusavice, *Phillips' Science of Dental Materials* (Elsevier Saunders, St. Louis, MO, 2003).
[19]S. Dumitriu, *Polymeric Biomaterials, Revised and Expanded* (Marcel Dekker, New York, 2001).
[20]R. Singla, P. Bogra, and B. Singal, J. Conserv. Dent. **15**, 233 (2012).
[21]R. M. Carvalho, A. P. Manso, S. Geraldeli, F. R. Tay, and D. H. Pashley, Dent. Mater. **28**, 72 (2012).
[22]Q. Ye, J. Park, J. S. S. Laurence, R. Parthasarathy, A. Misra, and P. Spencer, J. Dent. Res. **90**, 1434 (2011).
[23]Q. Ye *et al.*, Acta Biomater. **100B**, 1086 (2012).
[24]Y. Zou and J. L. P. Jessop, "Adhesive resin conversion and composition in the hybrid layer of the resin-dentin bond," Ph.D. dissertation (University of Iowa, Iowa City, IA, 2007).
[25]Y. Zou, S. R. Armstrong, and J. L. P. Jessop, J. Biomed. Mater. Res. Part A **94**, 288 (2010).
[26]Y. Wang, P. Spencer, and X. Yao, J. Biomed. Opt. **11**, 24005 (2006).
[27]Y. Wang and P. Spencer, J. Biomed. Mater. Res. Part A **59**, 46 (2002).
[28]P. Spencer and Y. Wang, J. Biomed. Mater. Res. **62**, 447 (2002).
[29]R. Parthasarathy, "Chemo-mechanical characterization of phase-separated dentin adhesives," Ph.D. dissertation (Ranganathan Parthasarathy, Lawrence, KA, 2013), see https://kuscholarworks.ku.edu/handle/1808/16797.
[30]A. Misra, P. Spencer, O. Marangos, Y. Wang, and J. L. Katz, J. Biomed. Mater. Res. Part B Appl. Biomater. **70**, 56 (2004).
[31]A. Misra, P. Spencer, O. Marangos, Y. Wang, and J. L. Katz, J. R. Soc. Interface **2**, 145 (2005).
[32]V. Singh, A. Misra, O. Marangos, J. Park, Q. Ye, S. L. Kieweg, and P. Spencer, Dent. Mater. **27**, e187 (2011).
[33]M. Nygårdsvoll, "Polymer based adhesives for tooth restorations. Monomer leakage and degradation," Thesis (University of Tromsø, Tromsø, Norway, 2010).
[34]J. De Munck, K. Van Landuyt, M. Peumans, A. Poitevin, P. Lambrechts, M. Braem, and B. Van Meerbeek, J. Dent. Res. **84**, 118 (2005).
[35]A. Misra, V. Singh, R. Parthasarathy, O. Marangos, and P. Spencer, *2011 IADR/AADR/CADR General Session*, San Diego, CA (2011).
[36]V. Singh, A. Misra, O. Marangos, J. Park, Q. Ye, S. Kieweg, and P. Spencer, J. Dent. Res. **90A**, e187 (2011).
[37]V. Singh, A. Misra, O. Marangos, J. Park, Q. Ye, S. L. Kieweg, and P. Spencer, J. Biomed. Mater. Res. Part B Appl. Biomater. **95**, 283 (2010).
[38]Y. Liu, L. Tjäderhane, L. Breschi, A. Mazzoni, N. Li, J. Mao, D. H. Pashley, and F. R. Tay, J. Dent. Res. **90**, 953 (2011).
[39]J. Malacarne, R. M. Carvalho, M. F. de Goes, N. Svizero, D. H. Pashley, F. R. Tay, C. K. Yiu, and M. R. O. Carrilho, Dent. Mater. **22**, 973 (2006).
[40]M. F. Ashby and D. R. H. Jones, *Engineering Materials 2: An Introduction to Microstructures and Processing* (Butterworth-Heinemann, Woburn, MA, 2012).
[41]R. Parthasarathy, A. Misra, J. Park, Q. Ye, and P. Spencer, J. Mater. Sci.: Mater. Med. **23**, 1157 (2012).
[42]F. Abedin, Q. Ye, H. J. H. J. Good, R. Parthasarathy, and P. Spencer, Acta Biomater. **10**, 3038 (2014).
[43]F. Abedin, Q. Ye, R. Parthasarathy, A. Misra, and P. Spencer, J. Dent. Res. **94**, 500 (2015).
[44]F. Abedin, Q. Ye, P. Spencer, R. Parthasarathy, J. S. Laurence, and A. Misra, "International association for dental research," *IADR/AADR/CADR General Session*, Seattle, WA, 22 March (2013).
[45]F. Abedin, Q. Ye, K. Camarda, and P. Spencer, J. Biomed. Mater. Res. Part B Appl. Biomater. **104**, 1666 (2015).
[46]Q. Ye, Y. Wang, and P. Spencer, J. Biomed. Mater. Res. B Appl. Biomater. **888**, 339 (2009).
[47]J. G. Park, Q. Ye, E. M. Topp, A. Misra, and P. Spencer, Dent. Mater. **25**, 1569 (2009).
[48]P. J. Flory, *Principles of Polymer Chemistry* (Cornell University, Ithaca, 1953).
[49]D. Chandler, Nature **437**, 640 (2005).
[50]A. D. McNaught and A. Wilkinson, *Compendium of Chemical Terminology* (Blackwell Science, Oxford, 1997).
[51]B. K. Fink, T. A. Bogetti, M. A. Stone, and J. W. Gillespie, Jr., Thermochemical response of vinyl-ester resin, DTIC Document, 2002.
[52]K. Matyjaszewski and T. P. Davis, *Handbook of Radical Polymerization*, 1st ed. (Wiley-Interscience, Hoboken, NJ, 2002).
[53]J. E. Mark and B. Erman, *Science and Technology of Rubber* (Academic, New York, 2011).
[54]A. Lappala, A. Zaccone, and E. M. Terentjev, Soft Matter **12**, 7330 (2016).
[55]A. Misra, R. Parthasarathy, Q. Ye, V. Singh, and P. Spencer, Acta Biomater. **10**, 330 (2014).
[56]P. H. Corkhill, A. M. Jolly, C. O. Ng, and B. J. Tighe, Polymer **28**, 1758 (1987).
[57]X. Ge, Q. Ye, L. Song, J. S. Laurence, and P. Spencer, JOM **67**, 796 (2015).
[58]L. Song, Q. Ye, X. Ge, A. Misra, C. Tamerler, and P. Spencer, RSC Adv. **6**, 52434 (2016).
[59]M. A. Bag and L. M. Valenzuela, Int. J. Mol. Sci. **18**, 1422 (2017).
[60]V. M. Gun'ko, I. N. Savina, and S. V. Mikhalovsky, Gels **3**, 37 (2017).
[61]I. Katime, E. D. de Apodaca, and E. Rodriguez, J. Appl. Polym. Sci. **102**, 4016 (2006).
[62]H. B. Lee, M. S. Jhon, and J. D. Andrade, J. Colloid Interface Sci. **51**, 225 (1975).

[63]S. Mani, F. Khabaz, R. V. Godbole, R. C. Hedden, and R. Khare, J. Phys. Chem. B **119**, 15381 (2015).
[64]S. Urata, J. Irisawa, A. Takada, W. Shinoda, S. Tsuzuki, and M. Mikami, J. Phys. Chem. B **109**, 4269 (2005).
[65]Y. Tamai, H. Tanaka, and K. Nakanishi, Macromolecules **29**, 6750 (1996).
[66]T.-X. Xiang and B. D. Anderson, Pharm. Res. **22**, 1205 (2005).
[67]H. Pessen and T. F. Kumosinski, *Methods Enzymol.* (Elsevier, New York, 1985), pp. 219–255.
[68]A. K. Denisin and B. L. Pruitt, ACS Appl. Mater. Interfaces **8**, 21893 (2016).
[69]R. M. Holt, Third EAGE Shale Workshop on Physics and Shale Chemistry, Copenhagen, 4–7 June 2012.
[70]J. M. G. Cowie and V. Arrighi, *Polymers: Chemistry and Physics of Modern Materials* (CRC, Boca Raton, FL, 2007).
[71]L. Brochard, M. Vandamme, and R.-M. Pellenq, J. Mech. Phys. Solids **60**, 606 (2012).
[72]C. Bauwens-Crowet, J. C. Bauwens, and G. Homes, J. Polym. Sci. Part A-2 Polym. Phys. **7**, 735 (1969).
[73]H. Eyring, J. Chem. Phys. **4**, 283 (1936).
[74]R. N. Haward and R. J. Young, *The Physics of Glassy Polymers* (Springer, Berlin, 1997).
[75]A. D. Mulliken, *Low to High Strain Rate Deformation of Amorphous Polymers: Experiments and Modeling* (Massachusetts Institute of Technology, Cambridge, MA, 2004).
[76]J. C. Bauwens, J. Mater. Sci. **7**, 577 (1972).
[77]J. A. Roetling, Polymer **6**, 311 (1965).
[78]J. A. Roetling, Polymer **6**, 615 (1965).
[79]Q. Ye, P. Spencer, Y. Wang, and A. Misra, J. Biomed. Mater. Res. Part A **80**, 342 (2007).
[80]J. N. Israelachvili, *Intermolecular and Surface Forces* (Academic, New York, 2011).
[81]S. Saw and P. Harrowell, Phys. Rev. Lett. **116**, 137801 (2016).
[82]H.-B. Yu, R. Richert, R. Maaß, and K. Samwer, Phys. Rev. Lett. **115**, 135701 (2015).
[83]R. Parthasarathy, A. Misra, and L. Ouyang, J. Phys. Condens. Matter **30**, 265901 (2018).
[84]R. Parthasarathy, A. Misra, S. Aryal, and L. Ouyang, Contin. Mech. Thermodyn. **30**, 1027 (2018).
[85]A. S. Hoffman, Adv. Drug Deliv. Rev. **64**, 18 (2012).
[86]L. C. Dong and A. S. Hoffman, J. Control. Release **4**, 223 (1986).
[87]A. K. Lele, M. M. Hirve, M. V. Badiger, and R. A. Mashelkar, Macromolecules **30**, 157 (1997).
[88]C. Tamerler, JOM **67**, 2480 (2015).
[89]S. Thomopoulos, V. Birman, and G. M. Genin, *Structural Interfaces and Attachments in Biology* (Springer, Berlin, 2012).
[90]G. M. Genin, A. Kent, V. Birman, B. Wopenka, J. D. Pasteris, P. J. Marquez, and S. Thomopoulos, Biophys. J. **97**, 976 (2009).
[91]J. Z. Wang, D. A. Dillard, and F. A. Kamke, J. Mater. Sci. **26**, 5113 (1991).
[92]V. Singh, A. Misra, R. Parthasarathy, Q. Ye, J. Park, and P. Spencer, J. Biomed. Mater. Res. Part B Appl. Biomater. **101**, 1437 (2013).
[93]P. Navi, V. Pittet, and C. J. G. Plummer, Wood Sci. Technol. **36**, 447 (2002).
[94]H. W. Haslach, Mech. Time-Dependent Mater. **4**, 169 (2000).
[95]J. Z. Wang, D. A. Dillard, and T. C. Ward, J. Polym. Sci. Part B Polym. Phys. **30**, 1391 (1992).
[96]A. Misra, R. Parthasarathy, V. Singh, and P. Spencer, Z. Angew. Math. Mech. **95**, 215 (2015).
[97]A. Misra, R. Parthasarathy, V. Singh, and P. Spencer, J. Nanomech. Micromech. **3**, 4013002 (2013).